VI
Strangeness

17 Thermal production of flavor in a deconfined phase

17.1 The kinetic theory of chemical equilibration

Strangeness, and more generally heavy-flavor quarks, can be produced either in the first interactions of colliding matter, or in the many ensuing less-energetic collisions. The mass of the strange quark $m_{\rm s}$ is comparable in magnitude to the typical temperatures reached in heavy-ion interactions, and the numerous 'soft' collisions of secondary partons dominate the production of strangeness, and naturally, of the light flavors u and d.

The masses of charm and bottom quarks are well above typical temperatures; these quarks are predominantly produced in the hard initial scattering. This process remains today a topic of current intense study both for the elementary and for the nuclear collisions [124]. We will not discuss it further in this book.

At the time at which the strange flavor approaches chemical equilibrium in soft collisions, the back reaction is also relevant. The quantum-mechanical matrix element driving a two-body reaction must be, channel by channel, the same for forward- and backward-going reactions. The actual rates of reaction differ since there are usually considerable differences in statistical and phase-space factors. However, the forward and backward reactions will balance when equilibrium yields of particles are established. This principle of detailed balance can sometimes be used to evaluate reaction rates.

The net change in yield of flavors f and $\bar{\rm f}$ is given by the difference between the rates of production and annihilation. The evolution in the density of heavy quarks in QGP can be described by the master equation

$$\frac{dN_{\rm f}(t)}{d^3x\,dt} = \frac{dN({\rm gg}, {\rm q\bar{q}} \to {\rm f\bar{f}})}{d^3x\,dt} - \frac{dN({\rm f\bar{f}} \to {\rm gg}, {\rm q\bar{q}})}{d^3x\,dt}. \tag{17.1}$$

https://doi.org/10.1017/9781009290753.024 Published online by Cambridge University Press

When locally at a point in space there is exact balance between the two terms on the right-hand side of Eq. (17.1), chemical equilibrium has been established, which, as we recall, is the state of maximum entropy; see section 7.1.

Each of the terms in Eq. (17.1) expresses a change in number of particles per unit of 4-volume and it is a Lorentz-invariant quantity. We take advantage of this to write

$$\partial_\mu j^\mu_{\rm f} \equiv \frac{\partial \rho_{\rm f}}{\partial t} + \frac{\partial \vec{v}\,\rho_{\rm f}}{\partial \vec{x}} = \rho^2_{\rm g}(t)\langle \sigma v\rangle_p^{\rm gg\to f\bar f} + \rho_{\rm q}(t)\rho_{\bar{\rm q}}(t)\langle \sigma v\rangle_p^{\rm q\bar q\to f\bar f} - \rho_{\rm f}(t)\rho_{\bar{\rm f}}(t)\langle \sigma v\rangle_p^{\rm f\bar f\to gg,q\bar q}. \tag{17.2}$$

The left-hand side describes the change in the local particle density including the effect of flow; the right-hand side is another way to express the change in number of particles in terms of individual reactions, as we shall show, see Eq. (17.7).

The momentum-averaged cross section of reacting particles is

$$\boxed{\langle \sigma v_{\rm rel}\rangle_p \equiv \frac{1}{1+I_{12}} \frac{\int d^3p_1 \int d^3p_2\, \sigma_{12} v_{12} f(\vec{p}_1) f(\vec{p}_2)}{\int d^3p_1 \int d^3p_2\, f(\vec{p}_1) f(\vec{p}_2)}.} \tag{17.3}$$

The factor $1/(1+I_{12})$ is introduced to avoid double counting of indistinguishable pairs of particles, $I_{12} = 1$ for an identical pair of bosons (gluons, pions), otherwise $I_{12} = 0$. Some authors introduce this factor into the kinetic equation Eq. (17.2). Considering that the cross section is obtained as an average over all reaction channels, the implicit sums over spin, color, and any other discrete quantum numbers can be combined in the particle density,

$$\boxed{\rho = \int \frac{d^3p}{(2\pi)^3} f(\vec{p}) = \int \frac{d^3p}{(2\pi)^3} \sum_{i={\rm s,c,...}} f_i(\vec{p}).} \tag{17.4}$$

We have suppressed, in the above discussion, the dependence of the phase-space distributions $f(\vec{p},\vec{x},t)$ on the spatial coordinates, as well as their evolution with time.

In general terms, we need to obtain $f(\vec{p},\vec{x},t)$ for gluons and light quarks from a solution of a transport master equation such as the Boltzmann equation. However, this introduces a large uncertainty due to our great ignorance of the early collision (quantum) dynamics. Moreover, a seven dimensional evolution equation for $f(\vec{p},\vec{x},t)$ cannot yet be handled with the available computing power without simplifying assumptions invoking spherical symmetry. Moreover, the uncertainty about the initial temperature, initial yield of strangeness from pre-equilibrium reactions, and the poorly known mass of the strange quark $m_{\rm s}$ introduce significant uncer-

https://doi.org/10.1017/9781009290753.024 Published online by Cambridge University Press

tainties into calculations of the yield of strangeness, and limit the need for very precise methods.

We proceed to simplify by the use of two assumptions, which follow from the discussion we presented in section 5.5.

- The kinetic (momentum-distribution) equilibrium is approached faster than the chemical (abundance) equilibrium [23, 231, 246]. This allows us to study only the chemical abundances, rather than the full momentum distribution of the (strange) quark flavor.
- Gluons equilibrate chemically significantly faster than does strangeness [276]. We consider the evolution of the population of strangeness only after gluons have (nearly) reached chemical equilibrium.

In view of these assumptions, the phase-space distribution $f_{\rm s}$ can be characterized by a local temperature $T(\vec{x},t)$ of a (Boltzmann) equilibrium distribution reached for $t\to\infty$, $f_{\rm s}^{\infty}$, with normalization set by a phase-space-occupancy factor:

$$f_{\rm s}(\vec{p},\vec{x};t)\simeq\gamma_{\rm s}(T)f_{\rm s}^{T}(p),\quad f_{\rm s}^{T}(p)=e^{-\sqrt{m_{\rm s}^2+p^2}/T}, \tag{17.5}$$

where $f_{\rm s}^{T}$ is the equilibrium Boltzmann momentum distribution. Equation (17.5) invokes in the momentum independence of $\gamma_{\rm s}$ the first assumption. The factor $\gamma_{\rm s}$ allows the local density of strange quarks to evolve independently of the local temperature.

Using the Boltzmann momentum distribution Eq. (17.5) in Eq. (17.3), we are performing a thermal average of the cross section and relative velocity, and the result is a thermally averaged cross section, a function that depends on T instead of $\sqrt{s}$. Some books refer to this as thermal reactivity; we will often call it the thermal cross section:

$$\langle\sigma v_{\rm rel}\rangle_T\equiv\frac{1}{1+I_{12}}\frac{\int d^3p_1\int d^3p_2\,\sigma_{12}v_{12}f_1^T(p)f_2^T(p)}{\int d^3p_1\int d^3p_2\,f_1^T(p)f_2^T(p)}. \tag{17.6}$$

This thermal cross section is dependent on T, and on the masses of reacting particles, and its physical dimension is volume per time. We will often drop the subscripts T and rel, since the only average to which we refer in a cross section is 'thermal', and, in this context, the velocity is always relative.

The thermal reaction rate per unit time and volume, $R_{12}(T)$, is obtained as follows: consider that a single particle '1' enters at velocity v_{12} a medium of particles '2'; the rate of reactions is $\langle\sigma v_{\rm rel}\rangle_T\rho_2$. If per unit volume there are N_1 particles, i.e., we have a density ρ_1, then

$$\boxed{R_{12}(T)\equiv\langle\sigma v_{\rm rel}\rangle_T\rho_1\rho_2.} \tag{17.7}$$

https://doi.org/10.1017/9781009290753.024 Published online by Cambridge University Press

The densities ρ_1 and ρ_2 arise from the momentum integration of the Boltzmann distributions f_1 and f_2, Eq. (17.4), and contain the degeneracy factors g_1 and g_2. This rate Eq. (17.7) is Lorentz invariant, i.e., all observers agree by how much the number of particles changes per (invariant) unit volume in space–time.

The following evaluation of R_{12} applies to reactions occurring in confined and deconfined matter. However, for almost all particles (except pions) in the hadronic gas, it is sufficient to use the Boltzmann momentum distribution function, since the phase-space cells are nearly empty, while the density of particles arises from the numerous resonances encountered (see section 12.1). In QGP, we must in general use the Bose and Fermi distributions, as appropriate, which will complicate the results slightly.

We recall here the (Mandelstam) variables s, t, and u characterizing, in an invariant way, the two-particle reaction $1 + 2 \to 3 + 4$,

$$s = (p_1 + p_2)^2 = (p_3 + p_4)^2, \tag{17.8a}$$

$$t = (p_1 - p_3)^2, \tag{17.8b}$$

$$u = (p_2 - p_3)^2, \tag{17.8c}$$

$$s + t + u = \sum_{i=1}^{4} m_i^2, \tag{17.8d}$$

where the 4-momenta $p^\mu = (E_p, \vec{p})$ are used with $E_p = \sqrt{\vec{p}^2 + m^2}$. $\sqrt{s}$ is as usual the total CM energy and t is the invariant generalization of the scattering angle.

The cross section for reaction of two particles to give n final-state particles is computed according to

$$\sigma_{12} v_{12} E_1 E_2 = \int \prod_{i=3}^{n+2} d^4 p_i \, \delta(p_i^2 - m_i^2) \Theta(p_i^0) \times \delta^4 \left(p_1 + p_2 - \sum_{i=3}^{n+2} p_i \right) |\mathcal{M}|^2. \tag{17.9}$$

$|\mathcal{M}(s,t)|^2$ is the reaction-matrix element obtainable, for perturbative processes, using the Feynman rules described in section 14.1. The relative velocity of two collinear particles, which is used in the definition of the cross section, is*

$$v_{12} 2E_1 2E_2 \equiv 2\lambda_2^{1/2}(s), = 2\sqrt{s - (m_1 + m_2)^2}\sqrt{s - (m_1 - m_2)^2}. \tag{17.10}$$

* $\lambda_2^{1/2}(s)$ has nothing to do with a fugacity.

https://doi.org/10.1017/9781009290753.024 Published online by Cambridge University Press

The invariant reaction rate, Eq. (17.7), thus is

$$R_{12} = \int \frac{d^3p_1}{(2\pi)^3 2E_1}\frac{d^3p_2}{(2\pi)^3 2E_2}\frac{f_1\, f_2}{1+I_{12}}\sigma_{12}v_{12}\times 2E_1\times 2E_2 \qquad (17.11)$$

$$= \frac{g_1 g_2}{(2\pi)^6}\int_{s_{\rm th}}^{\infty} ds\,\frac{2\lambda_2^{1/2}\sigma_{12}}{1+I_{12}}\left(\int\frac{d^3p_1}{2E_1}\frac{d^3p_2}{2E_2}e^{-E_1/T}e^{-E_2/T}\delta(s-(p_1+p_2)^2)\right),$$

where we have inserted a (dummy) integration over s. The lower limit $s_{\rm th}$ of the integration over s is the threshold for the reaction, usually $s_{\rm th} = (\sum_i m_i)^2$, the sum of masses of the final state created.

We are also interested in understanding at which values of $\sqrt{s}$ the production processes occur. We will evaluate the p_1 and p_2 momentum integrals first, which will leave us with a final integral over $\sqrt{s}$ in Eq. (17.11). We can present the rate of production as an integral over the differential rate dR_i/ds, where i refers to the reaction channel considered:

$$R \equiv \sum_i \int_{s_{\rm th}}^{\infty} ds\,\frac{dR_i}{ds} \equiv \sum_i \int_{s_{\rm th}}^{\infty} ds\,\sigma_i(s)P_i(s). \qquad (17.12)$$

$\sigma_i(s)$ is the cross section of the channel. The factor $P_i(s)$, which has the same dimension as the invariant rate R, is interpreted as the number of collisions per unit volume and time, and corresponds to the expression in the second line in Eq. (17.11), with the channel i corresponding to the collision of particles $\{1,2\}$.

In order to evaluate the p_1 and p_2 momentum integrals in Eq. (17.11), it is convenient to introduce, for the Boltzmann distributions, the 4-vector of temperature, Eq. (12.39), in the local restframe $\beta = (1/T, 0)$ and to write the (invariant) factor in large brackets in Eq. (17.11),

$$[\cdots] = \int d^4p_1\, d^4p_2\,\delta^4(p-p_1-p_2)\delta_0(p_1^2-m_1^2)\delta_0(p_2^2-m_2^2)$$
$$\times \int d^4p\, e^{-\beta\cdot p}\delta(p^2-s), \qquad (17.13)$$

with δ_0 being the δ-function restricted to positive roots of the argument only (compare with Eq. (12.45)). A dummy integration over $p = p_{\rm A} + p_{\rm B}$ allows one to rearrange the terms in a way that separates the expression into the two factor integrals. The first is known as the two particle invariant phase-space integral 'IMS2' [86]:

$$\int d^4p_1\, d^4p_2\,\delta^4(p-p_1-p_2)\delta_0(p_1^2-m_1^2)\delta_0(p_2^2-m_2^2) = \frac{\pi}{2}\frac{\sqrt{\lambda_2}}{s}. \qquad (17.14)$$

https://doi.org/10.1017/9781009290753.024 Published online by Cambridge University Press

$\lambda_2^{1/2}(s)$ is as defined in Eq. (17.10). The second integral can be obtained by evaluating Eq. (10.43), it appeared previously in Eq. (12.22):

$$\int d^4p e^{-\beta p}\delta_0(p^2-s) = \frac{2\pi}{\beta}\sqrt{s}K_1(\beta\sqrt{s}). \tag{17.15}$$

The invariant reaction rate, Eq. (17.7), is

$$\boxed{R_{12} = \frac{g_1 g_2}{32\pi^4}\frac{T}{1+I_{12}}\int_{s_{\rm th}}^{\infty} ds\,\sigma(s)\frac{\lambda_2(s)}{\sqrt{s}}K_1(\sqrt{s}/T).} \tag{17.16}$$

So far, we have not addressed the quantum nature of colliding particles. The difficult case is that of a pair of light quarks reacting at finite baryon density, for which one of the distributions cannot be expanded. Since, in this case, the mass of the light quark is negligible, one of the integrals can be done analytically. The integral of interest, which is obtained after performing the angular integrals in Eq. (17.11), is

$$K_1(\sqrt{s}/T) \to \frac{1}{T\sqrt{s}}\int_0^\infty dp_1\int_0^\infty dp_2\,\Theta(4p_1p_2-s)f_{\rm q}(p_1)f_{\bar{q}}(p_2), \tag{17.17}$$

with (compare with Eqs. (10.34a) and (10.34b))

$$f_{\rm q}(p) = \frac{1}{\gamma_{\rm q}^{-1}\lambda_{\rm q}^{-1}e^{p/T}+1}, \qquad f_{\bar{q}}(p) = \frac{1}{\gamma_{\rm q}^{-1}\lambda_{\rm q}e^{p/T}+1}.$$

Assuming that $\gamma_{\rm q}/\lambda_{\rm q} < 1$ (baryon-rich matter), we can expand the distributions for antiquarks and obtain the generalization of K_1 in Eq. (17.16):

$$K_1(\sqrt{s}/T) \to \sum_{l=1}^{\infty}(-)^{l+1}\frac{\gamma_{\rm q}^l}{l\lambda_{\rm q}^l}\int_0^\infty \frac{dp_1}{\sqrt{s}}\frac{\exp\left(-l\dfrac{s}{4Tp_1}\right)}{\gamma_{\rm q}^{-1}\lambda_{\rm q}^{-1}e^{p_1/T}+1}, \tag{17.18}$$

which has to be evaluated numerically.

In the special case that all chemical factors are unity (or otherwise allow the expansion), we expand Eq. (17.18) again to obtain

$$K_1(\sqrt{s}/T) \to \sum_{l,n=1}^{\infty}\frac{(\pm)^{l+n}}{\sqrt{s}\,l}\int_0^\infty dp_1\exp\left(-l\frac{s}{4Tp_1}-\frac{np_1}{T}\right). \tag{17.19}$$

We have allowed for Fermi and Bose distributions, recalling the expansion

$$\frac{1}{e^{E/T}\mp 1} = \pm\sum_{n=1}^{\infty}(\pm)^n e^{-nE/T}.$$

https://doi.org/10.1017/9781009290753.024 Published online by Cambridge University Press

The upper sign in Eq. (17.19) is for bosons and the lower for fermions. We now use

$$\int_0^\infty dx\, e^{-a/(4x)-bx} = \sqrt{\frac{a}{b}} K_1(\sqrt{ab}), \tag{17.20}$$

and obtain in the case $\gamma_q = \lambda_q = 1$ the generalization of K_1 in Eq. (17.16):

$$K_1(\sqrt{s}/T) \to \sum_{l,n=1}^{\infty} (\pm)^{l+n} \frac{K_1(\sqrt{lns}/T)}{\sqrt{ln}}. \tag{17.21}$$

We see how the powers of $\sqrt{s}$ cancel out, leaving only the slowly converging pre-factor. It turns out that many terms in the sum of l and n are required in order to arrive at a precise result.

17.2 Evolution toward chemical equilibrium in QGP

The conservation of current used in Eq. (17.2) applies to the laboratory 'Eulerian' formulation. This can also be written with reference to the individual particle dynamics in the so-called 'Lagrangian' description: consider ρ_s as the inverse of the small volume available to each particle. Such a volume is defined in the local frame of reference (subscript 'l') for which the local flow vector vanishes, $\vec{v}(\vec{x},t)|_{\rm local} = 0$. For the considered volume δV_l being occupied by a small number of particles δN (e.g., $\delta N = 1$), we have

$$\delta N_s \equiv \rho_s\, \delta V_l. \tag{17.22}$$

The left-hand side of Eq. (17.2) can be now written as

$$\frac{\partial \rho_s}{\partial t} + \frac{\partial \vec{v}\,\rho_s}{\partial \vec{x}} \equiv \frac{1}{\delta V_l}\frac{d\delta N_s}{dt} = \frac{d\rho_s}{dt} + \rho_s \frac{1}{\delta V_l}\frac{d\delta V_l}{dt}. \tag{17.23}$$

Since δN and $\delta V_l\, dt$ are Lorentz-invariant quantities, the actual choice of the frame of reference in which the right-hand side of Eq. (17.23) is studied is irrelevant and, in particular, it can be considered in the local rest frame. The last term in Eq. (17.23) describes the effect of volume dilution due to the dynamic expansion of matter. The other term on the right-hand side is then interpreted as the evolution of the local density in proper time of the volume element.

We continue to use the first form of Eq. (17.23) and evaluate the local change in number of particles. We introduce $\rho_s^\infty(T)$ as the (local) chemical-equilibrium abundance of strange quarks which arises at $t \to \infty$, thus $\rho_s = \gamma_s(t)\rho_s^\infty$. We use the Boltzmann equilibrium abundance, section 10.4,

$$\delta N_s = \delta V\, \gamma_s \rho_s^\infty = [T^3\, \delta V]\gamma_s \frac{3}{\pi^2}\, z^2 K_2(z). \quad z = \frac{m_s}{T}, \tag{17.24}$$

https://doi.org/10.1017/9781009290753.024 Published online by Cambridge University Press

In an entropy-conserving evolution, e.g., subject to (ideal) hydrodynamic flow, section 6.2, the first factor on the right-hand side in Eq. (17.24) (in square brackets) is a constant in time, $\delta V\, T^3 = \delta V_0\, T_0^3 =$ constant. We now substitute in Eq. (17.23) and obtain, using Eq. (10.54b),

$$\frac{\partial \rho_{\rm s}}{\partial t} + \frac{\partial \vec{v}\,\rho_{\rm s}}{\partial \vec{x}} = \dot{T}\rho_{\rm s}^{\infty}\left(\frac{d\gamma_{\rm s}}{dT} + \frac{\gamma_{\rm s}}{T} z \frac{K_1(z)}{K_2(z)}\right), \tag{17.25}$$

where $\dot{T} = dT/dt$. Only a part of the usual flow-dilution term is left, since we implemented the adiabatic volume expansion, and study the evolution of the phase-space occupancy in lieu of the particle density.

We include the collision term seen in Eq. (17.2) and two channels, the fusion of gluons and light-quark–antiquark fusion into a pair of strange (or equivalently charm) quarks:

$$\boxed{\begin{aligned}\dot{T}\rho_{\rm s}^{\infty}\left(\frac{d\gamma_{\rm s}}{dT} + \frac{\gamma_{\rm s}}{T} z \frac{K_1(z)}{K_2(z)}\right) = \gamma_{\rm g}^2(\tau) R^{\rm gg\to s\bar{s}} + \gamma_{\rm q}(\tau)\gamma_{\bar{q}}(\tau) R^{\rm q\bar{q}\to s\bar{s}} \\ -\gamma_{\rm s}(\tau)\gamma_{\bar{s}}(\tau)(R^{\rm s\bar{s}\to gg} + R^{\rm s\bar{s}\to q\bar{q}}).\end{aligned}} \tag{17.26}$$

Similar equations can be formulated for the evolution of $\gamma_{\rm g}$ and $\gamma_{\rm q}$. Knowledge of the dynamics of the local temperature, along with the required invariant rate of production $R(T)$, allows one to evaluate the dynamic behavior of occupancy fugacities $\gamma_i(t)$.

Since only weak interactions convert quark flavors, on the hadronic time scale we have $\gamma_{\rm s,q}(\tau) = \gamma_{\bar{\rm s},\bar{q}}(\tau)$. Moreover, detailed balance, arising from the time-reversal symmetry of the microscopic reactions, assures that the invariant rates for forward/backward reactions are the same, specifically

$$R^{12\to 34} = R^{34\to 12}, \tag{17.27}$$

and thus

$$\begin{aligned}\dot{T}\rho_{\rm s}^{\infty}\left(\frac{d\gamma_{\rm s}}{dT} + \frac{\gamma_{\rm s}}{T} z \frac{K_1(z)}{K_2(z)}\right) = \gamma_{\rm g}^2(\tau) R^{\rm gg\to s\bar{s}}\left(1 - \frac{\gamma_{\rm s}^2(\tau)}{\gamma_{\rm g}^2(\tau)}\right) \\ + \gamma_{\rm q}^2(\tau) R^{\rm q\bar{q}\to s\bar{s}}\left(1 - \frac{\gamma_{\rm s}^2(\tau)}{\gamma_{\rm q}^2(\tau)}\right).\end{aligned} \tag{17.28}$$

When all $\gamma_i \to 1$, the right-hand side vanishes; chemical equilibrium is established.

In order to be able to evolve the population of (strange) quarks we need to understand the population of gluons, i.e., $\gamma_{\rm g}$. Several workers have considered the glue approach to equilibrium in perturbative processes such as gluon splitting, e.g., gg → ggg [71, 252, 253, 275]. They find that, in the thermal environment, there is not enough production of gluons to reach chemical equilibrium. Accordingly, there are too few gluons to

https://doi.org/10.1017/9781009290753.024 Published online by Cambridge University Press

derive the approach to chemical equilibrium of light quarks, and, even more so, of strange quarks. The initial conditions for such a full-kinetic-evolution study are relatively unreliable, but can not alter this conclusion. We pursue an entirely different point of view in this book, based on the belief that strong multigluon processes $gg \to ng$, $n > 3$ can equilibrate the abundance of gluons faster [278]. Therefore, we assume that gluon chemical equilibrium is reached rapidly, $\mathcal{O}(1\,\mathrm{fm})$, on a scale not much longer than the time required to reach thermal equilibrium. Our choice of an initial condition for consideration of strange flavor equilibration is $\gamma_g = 1$. In the study of evolution of strange (and charm) quarks we also take $\gamma_q = 1$. A large error, in this last assumption, is without significance for what follows, since gluons dominate the thermal production of strange quarks.

Given the chemical equilibrium of gluons and light quarks, we obtain the dynamic equation describing the evolution of the local phase-space occupancy of strangeness (and, in analogy, charm),

$$2\tau_s \dot{T}\left(\frac{d\gamma_s}{dT} + \frac{\gamma_s}{T} z \frac{K_1(z)}{K_2(z)}\right) = 1 - \gamma_s^2. \tag{17.29}$$

As discussed at the end of section 5.7, we introduce the relaxation time τ_s of chemical (strangeness) equilibration as the ratio of the equilibrium density that is being approached and the rate at which this occurs,

$$\tau_s \equiv \frac{1}{2} \frac{\rho_s^\infty}{(R^{gg\to s\bar{s}} + R^{q\bar{q}\to s\bar{s}} + \cdots)}. \tag{17.30}$$

The factor $\frac{1}{2}$ is introduced by convention, in order for the quantity $\tau_s(T)$ to describe an exponential approach to equilibrium, Eq. (5.41).

One generally expects that $\gamma_s \to 1$ monotonically as a function of time. However, Eq. (17.29) allows the range $\gamma_s > 1$, for it incorporates the physics of a rapidly expanding high yield of strangeness created in the early stage at high T. At a high background temperature, the evolution $\gamma_s(t) \to 1$ produces a high yield of particles, which corresponds, at the lower temperature established after expansion of the system, to $\gamma_s > 1$. One finds that thermal annihilation of flavor cannot keep up with the rapid evolution of a fireball of QGP, and an overabundance will generally result. Annihilation is slow, since the density of strange and antistrange quarks is about four times smaller than the density of gluons (an effect of color and mass) and the rate of annihilation for strange quarks is 16 times slower. With a relaxation time for the production of strangeness of 1.5–10 fm (depending on temperature), see Fig. 17.11 below, the relaxation time for $s\bar{s}$ annihilation is 20–150 fm, so practically all strangeness is preserved on the time scale of 5 fm of a QGP fireball. For charm this argument is much stronger, given the greater effect of mass. Once it has been

https://doi.org/10.1017/9781009290753.024 Published online by Cambridge University Press

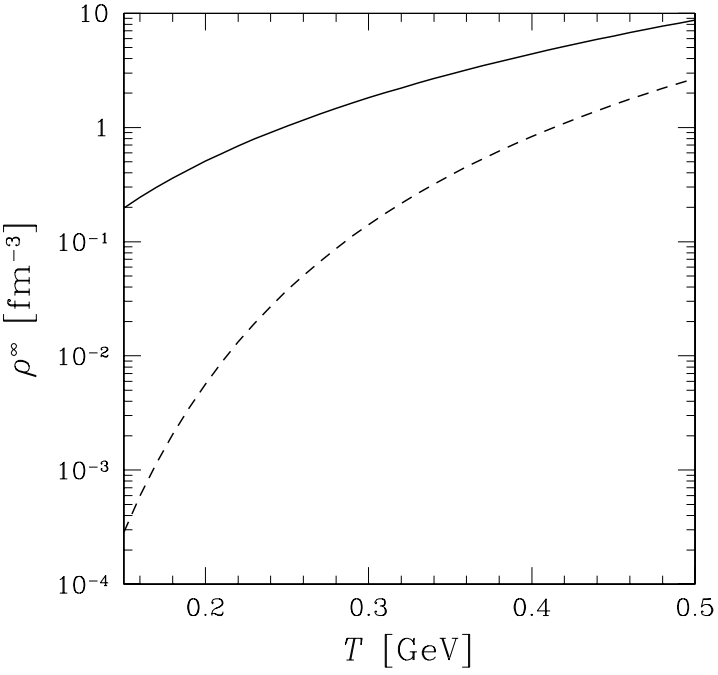

Fig. 17.1. The statistical equilibrium densities of strange or antistrange quarks with $m_{\rm s} = 160\,{\rm MeV}$ (solid line) and of charmed or anticharmed quarks with $m_{\rm c} = 1500\,{\rm MeV}$ (dashed line), as functions of temperature T.

produced, heavy flavor has no time to annihilate and reequilibrate. This is a very important feature that makes the yield of strangeness a 'deep' probe of the deconfined phase.

Said differently, the high abundance of strangeness (or charm) formed in the high-temperature QGP stage over-populates the available phase space at lower temperature, when the equilibration rate cannot keep up with the cooling due to expansion. We will quantify this effect in more detail in section 17.5. In the kinetic equation Eq. (17.29), this is seen most clearly by considering the case $T < m_{\rm s}$. In this limit, $1/\tau_{\rm s}$ becomes small, the dilution term (second term on the left-hand side in Eq. (17.29)) dominates the evolution of $\gamma_{\rm s}$. For the massive charm quarks $T \ll m_{\rm c}$, so expansion dilution can generate a very large phase-space overabundance, compared with the equilibrium yields expected in hadronization.

To grasp the sensitivity of these remarks to the early QGP stage, we look at the equilibrium densities of strange ($m_{\rm s} = 160\,{\rm MeV}$) and charmed ($m_{\rm c} = 1500\,{\rm MeV}$) quarks, shown in Fig. 17.1. We note that, for $T \simeq 250\,{\rm MeV}$, the equilibrium abundance of strangeness exceeds one $\bar{\rm s}$ quark for each fm^3 of matter, and that charm reaches this for $T \geq 450\,{\rm MeV}$.

https://doi.org/10.1017/9781009290753.024 Published online by Cambridge University Press

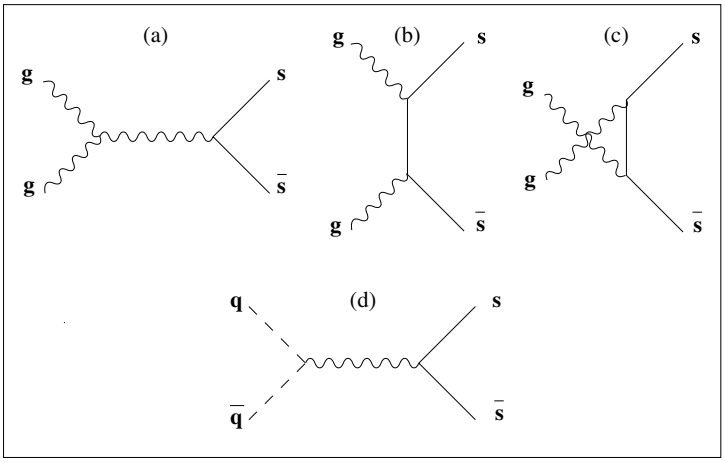

Fig. 17.2. Leading order Feynman diagrams for production of $s\bar{s}$ (and similarly $c\bar{c}$) by fusion of gluons and pairs of quarks ($q = u, d$).

Looking at charm, we note that, when the system expands and cools rapidly from $T = 450$ to 150 MeV, the volume grows by less than a factor of 70, see the entropy density in Fig. 16.7, while the equilibrium density of charm declines by factor 10 000 and the charm saturation factor γ_c increases by the factor 150, to preserve the yield of charm. This abundance of charm is a product of the first interactions, not of thermal processes, except possibly at the LHC in a very-high-T scenario.

17.3 Production cross sections for strangeness and charm

The production processes involving quark and gluon degrees of freedom in QGP are

$$u + \bar{u} \to s + \bar{s}, \qquad d + \bar{d} \to s + \bar{s}, \tag{17.31a}$$

$$g + g \to s + \bar{s}. \tag{17.31b}$$

These three processes describing perturbative production of pairs of strange quarks are represented to lowest order in Fig. 17.2, and have to be summed incoherently. These lowest-order diagrams were studied in the early eighties, for the quark process [68] and for the gluon process [226], employing fixed values of $\alpha_s = 0.6$ and $m_s = 160$–180 MeV.

The evaluation of the lowest-order Feynman diagrams shown in Fig. 17.2 yields the cross sections [95]:

$$\sigma_{q\bar{q}\to f\bar{f}}(s) = \frac{8\pi\alpha_s^2}{27s}\left(1+\frac{2m_f^2}{s}\right)w(s), \quad w(s) = \sqrt{1-\frac{4m_f^2}{s}}, \tag{17.32a}$$

https://doi.org/10.1017/9781009290753.024 Published online by Cambridge University Press

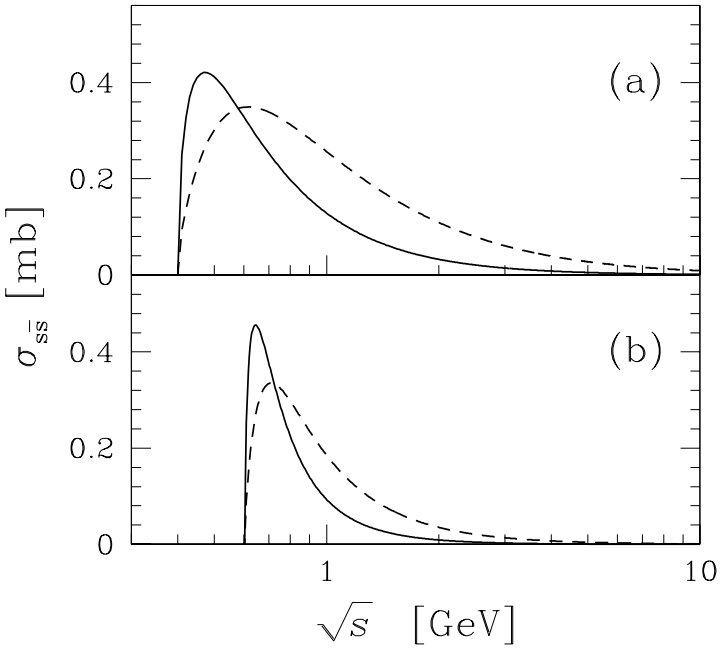

Fig. 17.3. Production cross sections for strangeness in leading order: (a) for $\alpha_s = 0.6$ and $m_s = 200\,\mathrm{MeV}$; (b) for running $\alpha_s(\sqrt{s})$ and $m_s(\sqrt{s})$, with $\alpha_s = 0.118$. Solid lines, $q\bar{q} \to s\bar{s}$; dashed lines, $gg \to s\bar{s}$.

$$\sigma_{gg\to f\bar{f}}(s) = \frac{\pi\alpha_s^2}{3s}\left[\left(1 + \frac{4m_f^2}{s} + \frac{m_f^4}{s^2}\right)\ln\left(\frac{1+w(s)}{1-w(s)}\right) - \left(\frac{7}{4} + \frac{31m_f^2}{4s}\right)w(s)\right]. \tag{17.32b}$$

Inspecting Fig. 17.3(a), we see that the magnitudes (up to 0.4 mb) of both types of reactions considered, quark fusion and gluon fusion, are similar. At this stage, it is not immediately apparent that gluons dominate the production of flavor.

The magnitude of the cross section of interest is normalized by α_s. To obtain Fig. 17.3(a), we took $\alpha_s = 0.6$. While the value seems reasonable, a value of $\alpha_s = 0.3$ would lengthen the relaxation time of strangeness, $\tau_s \propto \alpha_s^{-2}$, by a factor of four, nearly beyond the expected life span of the QGP fireball. Thus, we must improve the determination of α_s. There are two natural ways to do this; the easier one is to adopt the functional $\alpha_s(T)$ seen in Fig. 14.3. However, in such an approach, two-body collisions occurring at very different $\sqrt{s}$ but in a thermal bath at the same temperature T are evaluated with the same value of α_s. Only for the thermal production of

https://doi.org/10.1017/9781009290753.024 Published online by Cambridge University Press

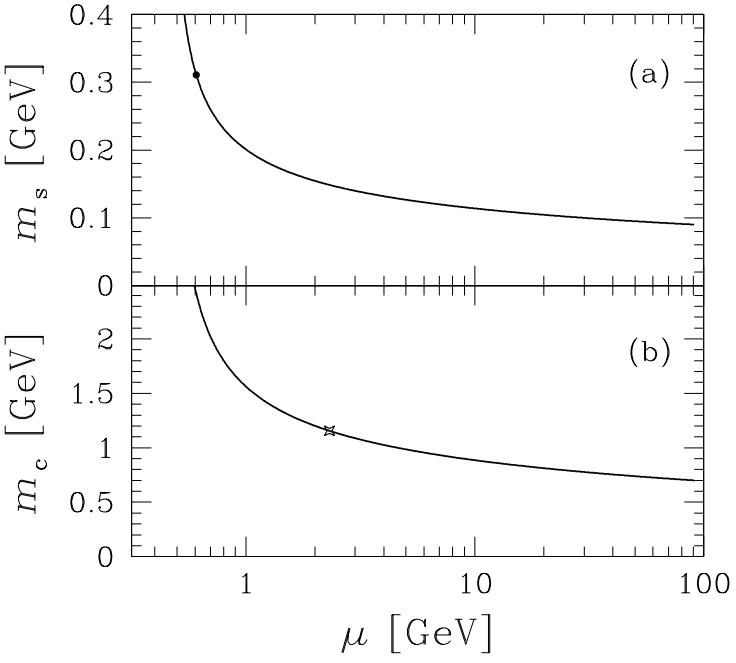

Fig. 17.4. Running masses for $\alpha_s = 0.118$: (a) the mass of the strange quark m_s, for which the dot indicates the production thresholds for pairs of strange quarks for $m_s(M_Z) = 90$ MeV; (b) the mass of the charmed quark m_c, for which the cross indicates production thresholds for pairs of charmed quarks for $m_c(M_Z) = 700$ MeV.

charm does this approach turn out to yield the same result as does the more complex, but more precise, consideration of an appropriate value of α_s for each collision, governed by the applicable $\alpha_s(\mu)$, Fig. 14.1, with $\mu \simeq \sqrt{s}$.

This second method, in which for each collision in the thermal bath an appropriate coupling strength is selected, is necessary for studying the production of strangeness in order to account for the growth of the cross section for soft scattering. The increase of cross section in soft collisions is, however, largely balanced by the concurrent suppression of the cross section due to the increase in mass of the strange quark m_s on the soft momentum scale. We adopt the running-mass and coupling-constant results presented in chapter 14, for $\alpha_s(M_Z) = 0.118$. In Fig. 17.4, the running masses of the strange and charm quarks $m_i(\mu)$, $i = \mathrm{s}, \mathrm{c}$, for $m_s(M_Z) = 90\,\mathrm{MeV}$ and $m_c(M_Z) = 700\,\mathrm{MeV}$, derived from Fig. 14.1, are shown. These values imply that $m_s(1\,\mathrm{GeV}) \simeq 200\,\mathrm{MeV}$ and $m_c(1\,\mathrm{GeV}) \simeq 1.55$ GeV.

https://doi.org/10.1017/9781009290753.024 Published online by Cambridge University Press

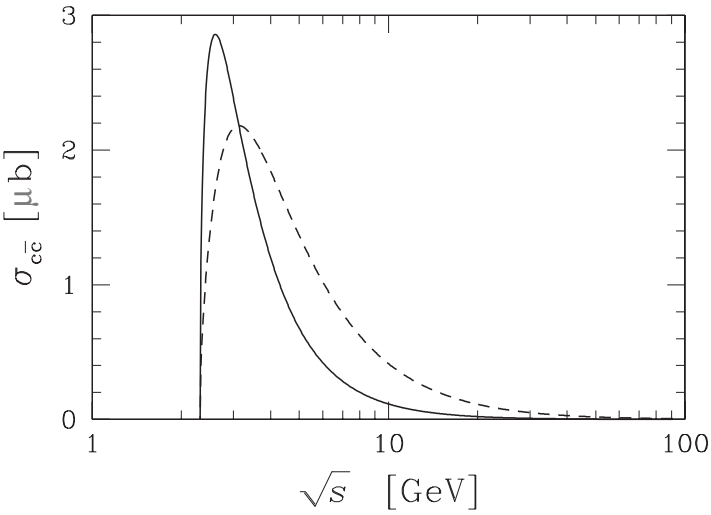

Fig. 17.5. Cross sections for leading order production of charm for the running α_s and running mass of the charmed quark with $m_c(M_Z) = 0.7\,\text{GeV}$: the solid line is for fusion of pairs of light quarks, whereas the dashed line is for $gg \to c\bar{c}$.

The energy scale of greatest interest for studying the production of strangeness is certainly $\mu = 2\pi T \simeq 1$–2 GeV, which is precisely the region of rapid change of the value of m_s. Below $\sqrt{s} = 1\,\text{GeV}$, the mass of the strange quark increases rapidly and the threshold for producing pairs of strange quarks increases to above $2m_s(1\,\text{GeV})$. Half of the threshold energy is indicated by the black dot in Fig. 17.4(a). The pair-production threshold is, section 14.4,

$$2m_s^{\text{th}}(\mu = 2m_s^{\text{th}}) = 611\,\text{MeV},\ m_s(M_Z) = 90\,\text{MeV},\ \alpha_s(M_Z) = 0.118.$$

For charm, the running-mass effect plays differently, since the naive threshold for production of charmed quarks $2m_c(2\,\text{GeV}) > 2\,\text{GeV}$. The running of the mass has the effect of reducing the effective threshold. For $m_c(M_Z) = 700\,\text{MeV}$, the production threshold is found, rather than at $3.1\,\text{GeV}$, at

$$2m_c^{\text{th}}(\mu = 2m_c^{\text{th}}) = 2.3\,\text{GeV},\ m_c(M_Z) = 700\,\text{MeV},\ \alpha_s(M_Z) = 0.118.$$

The cross, in Fig. 17.4(b), indicates the position of half of the threshold energy. Even this small reduction in threshold enhances the production of charm at low energy and especially so in the thermal environment we are considering.

In Fig. 17.3(b), we have presented the cross sections for production of strangeness Eqs. (17.32a) and (17.32b), evaluated using the running QCD parameters obtained in sections 14.3 and 14.4, identifying $\mu \to \sqrt{s}$.

https://doi.org/10.1017/9781009290753.024 Published online by Cambridge University Press

On comparing this with the 'conventional' result seen in Fig. 17.3(a), a greater threshold and more rapid decline of the cross sections are noted. Near $\sqrt{s} = 1$ GeV, in both cases, the fusion of gluons (dashed line) dominates, even though at lower energy the quark-pair fusion reaction (solid line) has a stronger peak. Similarly, for production of charm, we see in Fig. 17.5 the cross sections for fusion of gluons (dashed line) and pairs of quarks (solid line), for production cross sections which were computed for the running $\alpha_{\rm s}(M_{\rm Z}) = 0.118$ and running charmed-quark mass with $m_{\rm c}(M_{\rm Z}) = 700$ MeV. These cross sections are a factor 100 smaller than those for strangeness, at the level 1–2 μb. This is due to the fact that an eight-fold greater $\sqrt{s}$ is required, given that $\sigma \propto 1/s$, and a reduction in the effective coupling strength. The smallness of the cross section for production of charm is the reason why thermal production of charm becomes relevant only at $T \to 1$ GeV. Inspecting Fig. 17.5, we can also clearly understand the great sensitivity of the direct production of charm in non-thermal parton collisions to the value, and running, of the mass of the charmed quark: using a production threshold at 3 GeV, we cut 40% of the available strength of the cross section.

The use of scale dependent QCD parameters, $\alpha_{\rm s}$ and $m_{\rm f}$, ${\rm f} = {\rm s}, {\rm c}$, with $\mu \propto \sqrt{s}$ amounts to a re-summation of many QCD diagrams comprising vertex, and self energy corrections. A remaining shortcoming of thermal production evaluation is that up to day, there has not been a study of the next to leading order final state accompanying gluon emission in thermal processes, e.g., ${\rm gg} \to {\rm s\bar{s}} + {\rm g}$. In direct parton induced reactions, this next to leading order effect enhances the production rate by a factor $K = 1.5$–3. This causes a corresponding increase in the rate of production, and a reduction in the thermally computed chemical equilibration time of strangeness and charm.

17.4 Thermal production of flavor

The thermal production processes occur over a wide range of $\sqrt{s}$. There are two factors determining this. Aside from the cross section, the collision frequency is the determining factor. We have introduced the thermal collision frequency per unit time and volume $P_i(s)$ in channel i, Eq. (17.12). Employing the result Eq. (17.16) and the discussion of quantum corrections which followed, we obtain, setting $g_1 = g_2 = 16$, $I_{12} = 1$ and $\lambda_2 = s^2$ (for massless gluons)

$$P_{\rm g} = \frac{4Ts^{3/2}}{\pi^4} \sum_{l,n=1}^{\infty} \frac{1}{\sqrt{nl}} K_1\left(\frac{\sqrt{nl}\, s}{T}\right). \tag{17.33}$$

https://doi.org/10.1017/9781009290753.024 Published online by Cambridge University Press

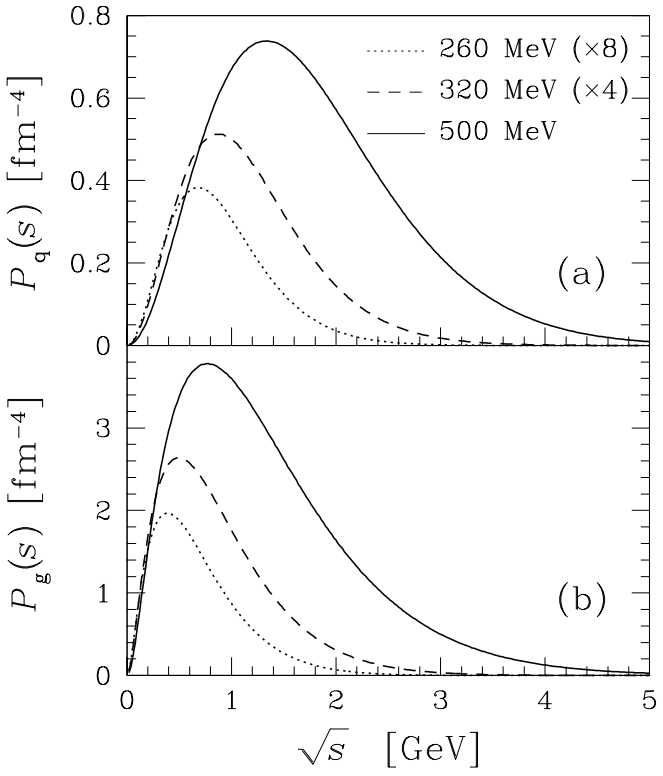

Fig. 17.6. The collision distribution functions as functions of $\sqrt{s}$: (a) for quarks and (b) for gluons, computed for temperature $T = 260\,\mathrm{MeV}$, $\lambda_q = 1.5$ (dotted lines, amplified by a factor of eight); $T = 320\,\mathrm{MeV}$, $\lambda_q = 1.6$ (dashed lines, amplified by a factor of four); and $T = 500\,\mathrm{MeV}$, $\lambda_q = 1.05$ (solid lines). In all cases $\gamma_q, \gamma_g = 1$.

For quark processes, using Eq. (17.18) for $\gamma_q/\lambda_q < 1$, and setting $g_1 = g_2 = 6$, $I_{12} = 0$ and $\lambda_2 = s^2$ (for massless quarks), and taking the result twice to allow for the two quark flavors which can undergo incoherent reactions,

$$P_q|_{\mu_q=0} = \frac{9Ts^{3/2}}{4\pi^4}\sum_{l=1}^{\infty}(-)^{l+1}\frac{\gamma_q^l}{l\lambda_q^l}\int_0^\infty \frac{dp_1}{\sqrt{s}}\frac{\exp\left(-l\dfrac{s}{4Tp_1}\right)}{\gamma_q^{-1}\lambda_q^{-1}e^{p_1/T}+1}. \quad (17.34)$$

In Fig. 17.6, the distribution functions for the collision frequency Eqs. (17.33) and (17.34) are presented as functions of $\sqrt{s}$ for gluons (b), and a $q\bar{q}$ pair of light quarks (a). The temperatures correspond to a range of possible initial fireball temperatures at the SPS and RHIC: $T = 260$ MeV (dotted, $\lambda_q = 1.5$), 320 MeV (dashed, $\lambda_q = 1.6$), and 500 MeV

https://doi.org/10.1017/9781009290753.024 Published online by Cambridge University Press

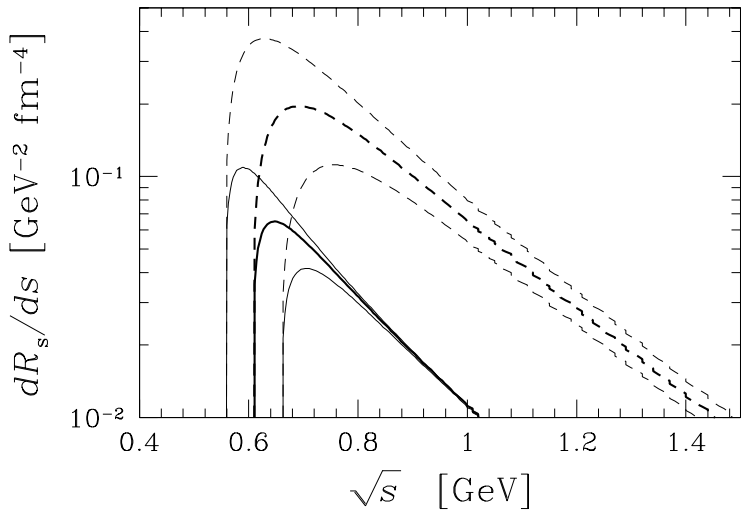

Fig. 17.7. The differential thermal production rate for strangeness dR_s/ds, with $T = 250$, $\lambda_q = 1.5$ for gluons (dashed line), and $q\bar{q} \to s\bar{s}$ (solid line, includes two interacting flavors), for the running $\alpha_s(M_Z) = 0.118$ and running mass of the strange quark $m_s(M_Z) = 90$ MeV $\pm$ 20% (thin lines).

(solid $\lambda_q = 1.05$). Gluons and light quarks are assumed to be in chemical equilibrium, $\gamma_q, \gamma_g = 1$.

There is a shift in the maximum of the distribution of $P_{q,g}$ to higher $\sqrt{s}$ with increasing temperature. The collision frequency for gluons is about five times greater, $P_g \simeq 5P_q$, than that for a pair of quarks, and this is the origin of the glue dominance of thermal production of strangeness. Moreover, the peak in the gluon collision frequency P_g is more coincident with the peak in the cross section, as a function of $\sqrt{s}$, Fig. 17.3(b). This further amplifies the gluon dominance. This combined enhancement effect can be seen in the thermal differential production rates,

$$\frac{dR_f}{ds} = \sum_{i=q,g} \sigma_f^i(s) P_i(s), \qquad f = s, c, \tag{17.35}$$

shown for thermal production of strangeness, in Fig. 17.7 for $T = 250$ MeV, and for thermal production of charm, in Fig. 17.8 for $T = 500$ MeV. Gluons (dashed lines) dominate quark-pair processes (solid lines), which are contributing at the level of 15%. The uncertainty in mass of the strange quark has significant impact; thin lines bordering thick lines show the effect of 20% variation in the value of the quark mass considered.

Since formation of charm occurs in the domain $T \ll m_c$, near to the threshold, where the cross section for fusion of a pair of quarks dominates gluon fusion, the gluon dominance of the production rate is not

https://doi.org/10.1017/9781009290753.024 Published online by Cambridge University Press

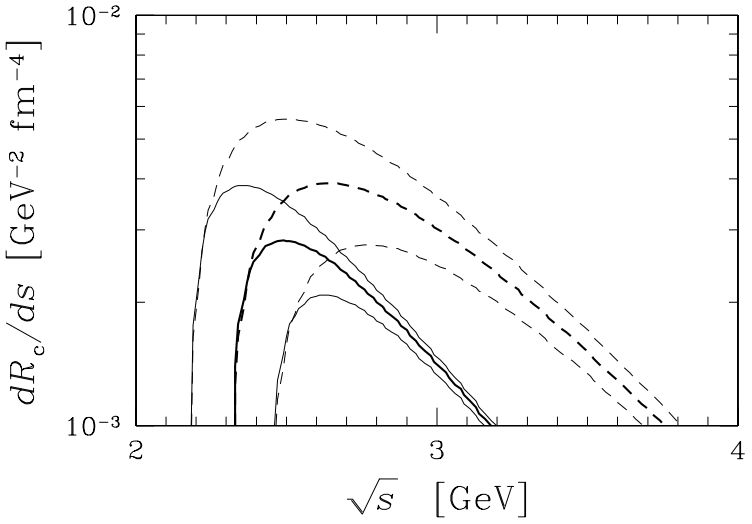

Fig. 17.8. The differential thermal production rate for charm dR_c/ds, with $T = 500\,\text{MeV}$, $\lambda_q = 1$ for gluons (dashed lines) and $q\bar{q} \to c\bar{c}$ (solid line, includes three interacting flavors), for the running $\alpha_s(M_Z) = 0.118$ and running mass of the charmed quark $m_c(M_Z) = 700$ MeV $\pm$ 7% (thin lines).

as pronounced as it is for strangeness. Only for $T \geq 500\,\text{MeV}$ does the glue fusion pick up strength and clearly dominate the thermal production of charm. Yet, even at $T = 500$ MeV, the rates for charm are a factor 100 smaller than those for strangeness at $T = 250$ MeV, and thermal production of charm is expected to be irrelevant at the RHIC.

The differential production rate can easily be integrated, and we show the results in Fig. 17.9 for strangeness, and in Fig. 17.10 for charm. In Fig. 17.9, we see that the early results (dotted line) [226] are found within the uncertainty in mass of the strange quark (a smaller mass leads to a bigger value of R). A yet greater value of R should result after the K-factor has been introduced, describing the next-to-leading-order effects. The rate of production of strangeness per unit volume and time is at the level of unity at temperatures reached at the RHIC, and production of strangeness is very abundant.

The thermal production of charm could be significant at the LHC relative to the direct first-parton-collision production, if temperatures well above $T = 500$ MeV are reached. We see, in Fig. 17.10, that the production rate for charm changes by six orders of magnitude as the temperature varies between 200 and 600 MeV. This sensitivity to the initial temperature is due to the exponential suppression with $m/T > 1$. In turn, this implies that the thermal production of charm can become important at sufficiently high temperature.

https://doi.org/10.1017/9781009290753.024 Published online by Cambridge University Press

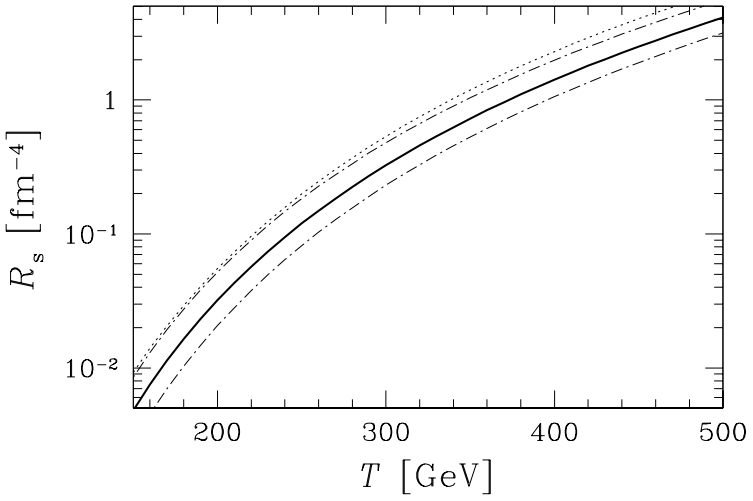

Fig. 17.9. Thermal production rates for strangeness R_s in QGP (thick solid line), calculated for $\lambda_q = 1.5$, $\alpha_s(M_Z) = 0.118$, and $m_s(M_Z) = 90$ MeV, as a function of temperature. Chain lines show the effect of variation of the mass of the strange quark by 20%. The dotted line shows comparison results for fixed $\alpha_s = 0.6$ and $m_s = 200\,\mathrm{MeV}$.

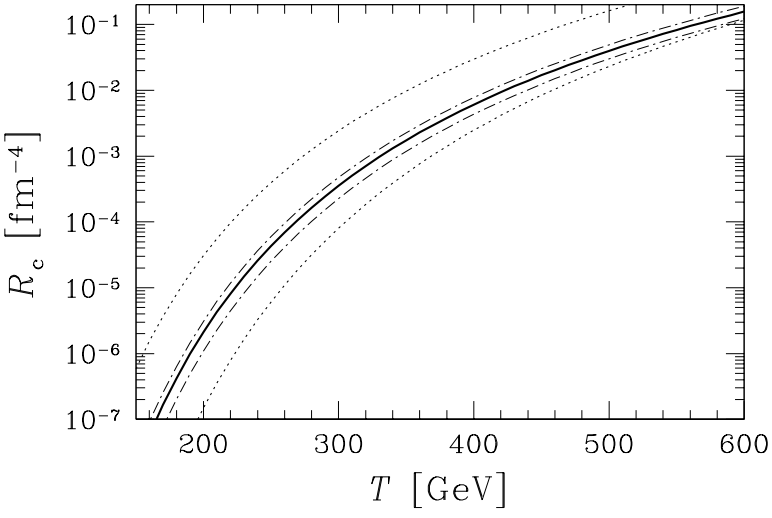

Fig. 17.10. Thermal production rates for charm R_c in QGP (solid line), calculated for $\lambda_q = 1.05$, $\alpha_s(M_Z) = 0.118$, and $m_c(M_Z) = 0.7\,\mathrm{GeV}$, as a function of temperature. Chain lines show the effect of variation of mass of the charmed quark by 7%. Dotted lines are comparison results for fixed $\alpha_s = 0.35$ and $m_c = 0.9\,\mathrm{GeV}$ (upper) and $\alpha_s = 0.4$ and $m_c = 1.5\,\mathrm{GeV}$ (lower).

https://doi.org/10.1017/9781009290753.024 Published online by Cambridge University Press

Insertion of the rates R_i into Eq. (17.30) allows us to obtain the time constants for chemical relaxation τ_s and τ_c. It should be stressed that, in an actual kinetic evaluation of the production of flavor, the relaxation time τ_f enters only when we relate the actual yield of flavor to the expected yield ρ_f^∞. Namely, the back reaction, $f\bar{f} \to gg, q\bar{q}$, is driven by the actual density of strangeness, whereas the forward rate, ignoring Pauli blocking, is not affected by the equilibrium yield at all. Which m_f is used in Eq. (17.30) to define ρ_f^∞ is physically irrelevant, as long as the same values of m_f and ρ_f^∞ are used both in the definition of τ_f, Eq. (17.30), and in $\gamma_f(t) = \rho_f/\rho_f^\infty$. In Fig. 17.11, we see τ_s evaluated with $m_s(1\text{GeV}) = 200$ MeV. The range of the assumed 20% uncertainty in $m_s(M_Z)$ is indicated by the hatched areas. The initial predictions obtained 20 years ago [226] at fixed values $\alpha_s = 0.6$ and $m_s = 200$ MeV (the dotted line in Fig. 17.11) are well within the band of values related to the uncertainty in mass of the strange quark. The approximate formula obtained in [226],

$$\tau_f = \frac{1.6}{\alpha_s^2 \gamma_g^2 T} \frac{m_f/T\, e^{m_f/T}}{[1 + (99/56)T/m_f + \cdots]}, \tag{17.36}$$

allows a quick estimate of the expected relaxation time in all the environments discussed in this subsection. We have added the pre-factor γ_g^{-2} relevant in case the dominant source of heavy flavor, gluons, is not in chemical equilibrium. We see that the equilibration time lengthens accordingly.

Thermal nonperturbative effects on the relaxation of strangeness were studied by introducing thermal, temperature-dependent, particle masses [70]. After the new production rates, including the now possible gluon decay, were added up, the total rate of production of strangeness was found to be little changed compared with the free-space rate. This finding was challenged [34], but a further reevaluation [66] confirmed that the rates obtained with perturbative glue-fusion processes are describing precisely the rates of production of strangeness in QGP, for the relevant temperature range $T > 200$ MeV. We can thus assume today that the 'prototype' strangeness-production processes seen in Fig. 17.2, re-summed using the renormalization-group method, are dominating the rates of production of strangeness in QGP.

The poor knowledge about the mass of the strange quark makes it possible that the actual relaxation time for strangeness is even smaller. In quenched-lattice calculations, see section 15.5, a much smaller value $m_s(M_Z) \lesssim 50$ MeV is found. The thin-dotted line in Fig. 17.11 gives the corresponding result for $m_s(M_Z) = 50$ MeV. We see that the relaxation time is already small enough to allow chemical equilibration at $T < 200$ MeV. Moreover, next-to-leading-order effects (the K-factor) should further reduce the chemical relaxation constant.

https://doi.org/10.1017/9781009290753.024 Published online by Cambridge University Press

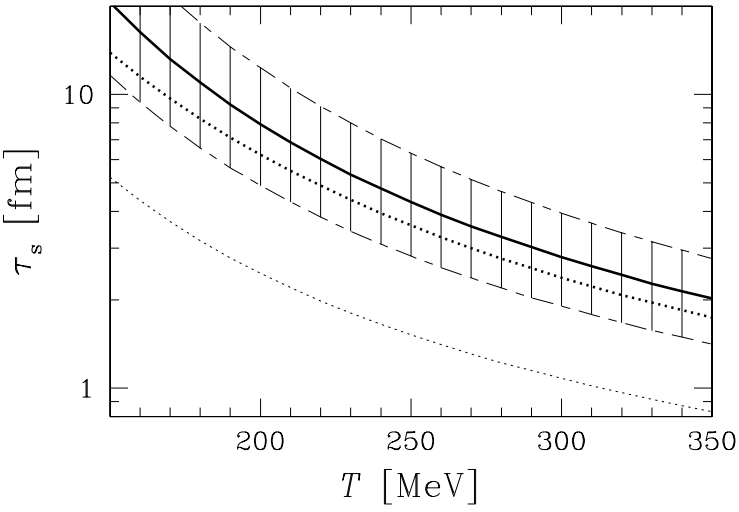

Fig. 17.11. The QGP chemical relaxation time for strangeness τ_s, for $\alpha_s(M_Z) = 0.118$ with $m_s(M_Z) = 90$ MeV and $\rho_s^\infty(m_s \simeq 200\,\mathrm{MeV})$ (thick line). Hatched areas show the effect of variation of the mass of the strange quark by 20%. The fat-dotted line shows comparison results for fixed $\alpha_s = 0.6$ and $m_s = 200\,\mathrm{MeV}$. The thin-dotted line shows the result for $m_s(M_Z) = 50$ MeV.

While precise evaluation of the production of strangeness at temperatures as low as $T_c \simeq 160$ MeV is not reliable within the scheme we have presented, it is highly probable that the combined effect of low m_s and the K-factor would ensure that near-chemical equilibrium for strangeness can develop as soon as the QGP phase can be formed. As a result, the strangeness energy excitation function, seen in Fig. 1.5 on page 17, can then be interpreted as due to the onset of deconfinement already in collisions below SPS energies. We see that, despite 20 years' work on strangeness, we still have many new, interesting insights to gain.

In Fig. 17.12, the chemical relaxation time for charm is shown in the extended interval through $T = 1000$ MeV. Since charm is considerably more massive than strangeness, there is less uncertainty in the extrapolation of the running QCD coupling constant. There is also less relative uncertainty in the value of the mass of the charmed quark, shown by the hatched area. We also see (dotted lines) the results for fixed m_c and α_s with parameters selected to border high- and low-T limits of the results presented. In the high-T limit, the choice (upper dotted line) $m_c = 1.5\,\mathrm{GeV}$, $\alpha_s = 0.4$ is appropriate, whereas to follow the result at small T (lower dotted line), we take a much smaller mass $m_c = 0.9\,\mathrm{GeV}$, with $\alpha_s = 0.35$.

The important result, see Fig. 17.12, is that, above $T = 700$ MeV, the relaxation time drops below to 10 fm; the curves flatten. At gluon

https://doi.org/10.1017/9781009290753.024 Published online by Cambridge University Press

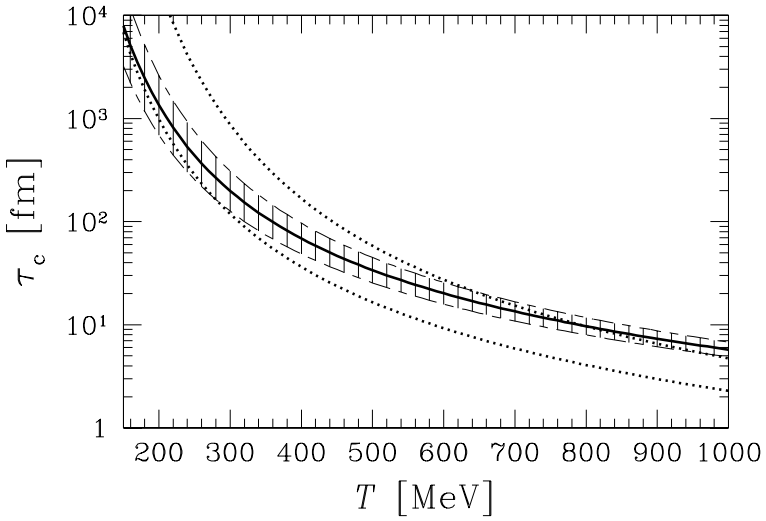

Fig. 17.12. Solid lines show the thermal relaxation constant for charm in QGP, calculated for running $\alpha_s(M_Z) = 0.118$, $m_c(M_Z) = 0.7\,\text{GeV}$ and $\rho_c^\infty(m_c \simeq 1.5\,\text{GeV})$. Lower dotted line, for fixed $m_c = 0.9\,\text{GeV}$ and $\alpha_s = 0.35$; upper dotted line, for fixed $m_c = 1.5\,\text{GeV}$ and $\alpha_s = 0.4$. The hatched area shows the effect of variation $m_c(M_Z) = 0.7\ \text{GeV} \pm 7\%$.

collision energies of several GeV, it is quite natural to expect that the next-to-leading-order effects enhance the cross section for production of charm by a factor of two, and this reevaluated relaxation time would correspond to a true value of a few fermis only. At this juncture in time, it is quite impossible to be sure how important the thermal component is in the production of charm at the LHC. On the other hand, even the first parton collisions are expected to produce $200 \pm 50\%$ $c\bar{c}$ pairs, and thus, in one way or another, charm certainly will be the novel-physics frontier at LHC energies, replacing strangeness as the flavor signature of new physics.

17.5 Equilibration of strangeness at the RHIC and SPS

Given the relaxation constant τ_s, we evaluate the thermal yield of strangeness in the QGP which arises on integrating the kinetic equation Eq. (17.29). Since this requires as input initial conditions the temporal evolution of the fireball, results are somewhat model-dependent. Indeed, there is considerable difference of opinion among groups regarding the well-studied RHIC system [71, 221, 252, 253, 275], since the experimental data which would narrow down the models is only now being obtained. The most important issue on which the various groups differ is the directly

https://doi.org/10.1017/9781009290753.024 Published online by Cambridge University Press

(or indirectly) assumed gluon content. In this book, we assume rapid chemical equilibration of gluons, which is not reached in studies relying on kinetic evolution by implementing the lowest-order gg → ggg gluon fragmentation.

For the RHIC conditions, we present a qualitative model with a cylindrical longitudinal flow, and transverse expansion [221]. We assume that the transverse flow of matter occurs at the velocity of sound for relativistic matter $v_\perp \simeq c/\sqrt{3} = 0.58c$. For a purely longitudinal expansion, the local entropy density scales according to $S \propto T^3 \propto 1/\tau$; see Eqs. (6.35) and (7.22). The transverse flow of matter accelerates the drop in entropy density. To model this behavior without too great a numerical effort, considering the other uncertainties, the following temporal-evolution function of the temperature was proposed:

$$T(\tau) = T_0 \left(\frac{1}{(1 + 2\tau c/d)(1 + \tau v_\perp / R_\perp)^2} \right)^{1/3}. \tag{17.37}$$

Considering various values of T_0, the temperature at which the gluon equilibrium is reached, the longitudinal dimension is scaled according to

$$d(T_0) = (0.5\,\mathrm{GeV}/T_0)^3 \times 1.5\,\mathrm{fm}. \tag{17.38}$$

This adjustment of the initial volume V_0 assures that the different evolution cases refer to a fireball with a similar entropy content. The following results are thus a study of one and the same collision system, and the curves reflect the uncertainty associated with unknown initial conditions of a fireball of QGP with identical, (but large by current standards) entropy content.

The numerical integration of Eq. (17.29) is started at $\tau_0 = 1$ fm/c, the time at which thermal initial conditions are reached. A range of initial temperatures 300 MeV $\leq T_0 \leq$ 600 MeV, varying in steps of 50 MeV, is considered. Since the initial p–p collisions also produce strangeness, to estimate the initial abundance a common initial value $\gamma_s(T_0) = 0.15$ is used. For $T_0 = 0.5$ GeV, the thickness of the initial collision region is $d(T_0 = 0.5)/2 = 0.75$ fm. The initial transverse dimension in nearly central Au–Au collisions is taken to be $R_\perp = 4.5$ fm. The initial volume of QGP is 190 fm^3, which, at the temperature of $T_0 = 0.5$ GeV, implies, according to results seen in Fig. 16.7, a total entropy content of $S =$ 38 000. We divide this by the specific entropy content per hadron in the final state, $S/N = 4$; see section 10.6. We see that the primary final-state hadron multiplicity has implicitly been assumed to be 9500. This is somewhat above results seen even during the RHIC run at $\sqrt{s_N} = 200$ GeV, for which we estimate, for the 3% most central events, a total hadron multiplicity, after resonance cascading, of 8000.

https://doi.org/10.1017/9781009290753.024 Published online by Cambridge University Press

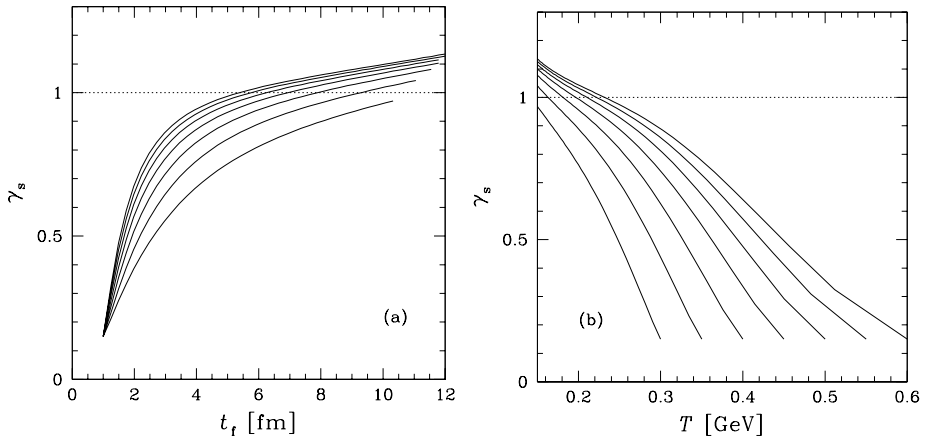

Fig. 17.13. The evolution of QGP phase-space occupancy for strangeness γ_s: (a) as a function of time and (b) as a function of temperature for $m_s(1\,\mathrm{GeV}) = 200\,\mathrm{MeV}$; see the text for details.

The evolution with time in the plasma phase is followed up to the breakup of the QGP at a temperature $T_f^{\mathrm{RHIC}} \simeq 150 \pm 5$ MeV. The numerical solution of Eq. (17.29) for γ_s is shown as a function both of time t, in Fig. 17.13(a), and of temperature T, in Fig. 17.13(b). This evolution is physically meaningful until it reaches the QGP breakup condition. Since the results for higher temperatures are also displayed, the reader who prefers hadronization at $T = 170 \pm 5$ MeV can easily draw his own conclusions.

We see in Fig. 17.13 the following phenomena.

- A steep rise at early times, showing actual production of strangeness, which is followed by a dilution-driven increase of γ_s near the breakup temperature.
- Widely different initial conditions (but with similar initial entropy contents) lead to rather similar chemical conditions at chemical freeze-out of strangeness.
- Despite the use of a high mass of $m_s = 200$ MeV, we find that strangeness nearly equilibrates chemically, and that the dilution effect allows in certain cases a small over-population of the strange-quark phase space even in the strangeness-dense QGP.
- For a wide range of initial conditions and final freeze-out temperature a narrow band of final result is seen, $1.10 > \gamma_s(T_f) > 0.9$.

Since strangeness is more easily made in the 'hot' era in glue–glue interactions, we can estimate that, if the abundance of glue had been at the time 70% chemically equilibrated, then $\gamma_s \simeq 0.5$. This high sensitivity to

https://doi.org/10.1017/9781009290753.024 Published online by Cambridge University Press

the glue density is at the origin of the claim that measuring the yield of strangeness probes the presence and abundance of glue, which is a specific property of QGP.

In the model calculations presented, the fireball begins to expand in the transverse direction instantly at the full velocity. For this reason, the initial drop in temperature is very rapid. This defect also makes the transverse size at the end of the expansion too large, $R_\perp \simeq R_0 + t_f/\sqrt{3} \simeq 9$ fm, compared with the results of HBT analysis, Fig. 9.11. This can easily be fixed by introducing a more refined model of the transverse velocity, which needs time to build up. The yield of strangeness may slightly increase in such a refinement, since the fireball will spend more time near to the high initial temperature.

The RHIC results presented are typical for all collision systems. In the top SPS energy range, the initial temperature reached is certainly less (by 10%–20%) than that in the RHIC 130-GeV run, and the baryon number in the fireball is considerably greater; however, the latter difference matters little for production of strangeness, which is driven by gluons. A model similar to the above yields $\gamma_{\rm s}^{\rm QGP} \simeq 0.6$–$0.7$, the upper index reminds us that in this section the strangeness occupancy factor $\gamma_{\rm s}$ refers to the property of the deconfined phase. The experimental observable directly related to $\gamma_{\rm s}^{\rm QGP}$ is the total yield of strangeness per participating baryon. We will return to discuss the significance of these results in section 19.4.

18 The strangeness background

18.1 The suppression of strange hadrons

Since the matter around us does not contain valence strange quarks, all strange hadrons produced must contain newly made strange and antistrange quarks. If strangeness is to be used as a diagnostic tool for investigating QGP, we need to understand this background rate of production of strange hadrons. In that context, we are interested in measuring how often, compared with pairs of light quarks, strange quarks are made. One defines for this purpose the strangeness-suppression factor[†]

$$W_{\rm s} = \frac{2\langle {\rm s}\bar{\rm s}\rangle}{\langle {\rm u}\bar{\rm u}\rangle + \langle {\rm d}\bar{\rm d}\rangle}. \tag{18.1}$$

In $W_{\rm s}$, all newly made $\rm s\bar{s}$, $\rm u\bar{u}$, and $\rm d\bar{d}$ quark pairs are counted.

If strangeness were to be as easily produced as light u and d quarks, we would find $W_{\rm s} \to 1$. To obtain the experimental value for $W_{\rm s}$, a careful study of produced hadron yields is required [277]. Results shown in

[†] We chose $W_{\rm s}$ in lieu of the usual symbol $\lambda_{\rm s}$, which clashes with the strangeness fugacity.

https://doi.org/10.1017/9781009290753.024 Published online by Cambridge University Press